Spatio-temporal assessment of aerosol-induced atmospheric heating rates in Nigeria

Tertsea Igbawua[ID]*, Aondongu Alexander Tyovenda, Terver Sombo, Idugba Mathias Echi

aDepartment of Physics, Joseph Sarwuan Tarka University, Makurdi, Benue State, Nigeria

Abstract

Understanding the dynamics of atmospheric heating rates (AHR) is crucial for assessing the impact of aerosols on Earth's energy balance and consequently, on climate dynamics. This study investigates the spatial and temporal patterns of AHR across Nigeria from 2000 to 2022, using a radiative transfer model. Detrended Fluctuation Analysis (DFA) and Ordinary Least Squares Regression (OLR) were employed to assess the persistence of AHR over time. The Mann-Kendall test was applied to identify trends in AHR and other related variables, while causal relationships between AHR and influencing aerosol variables were examined using Transfer Entropy (TE) analysis. The national average AHR was 0.77±0.15 K/day, with an insignificant decreasing trend from 2000 to 2022. The AHR distribution correlated with aerosol optical depth (AOD) in all climate zones except BSh and BWh. In zones with persistent substantial and marginal decreases in AHR, sea salt (SS) and desert dust (DU) were the dominant variables, with the highest TE values of 0.155 and 0.179, respectively. Findings show that monthly aerosol absorption (Single Scattering Albedo (SSA) <0.89) was prevalent only in the Csb climate zone between November and February, while other zones remained dominated by aerosol scattering (SSA > 0.89). This suggests the essential role of scattering aerosols in limiting AHR, especially during the rainy season. The aerosol absorption by coarse-mode aerosols was more dominant in northern Nigeria compared to mixed-mode aerosol absorption. Seasonally, the mixed-aerosol mode dominated in southern Nigeria during the December-January-February (DJF), June-July-August (JJA), and September-October-November (SON) seasons. This study provides insights into the complex dynamics of AHR, with important consequences for climate and atmospheric processes across different regions and seasons.

Communicated by: B. J. Falaye

1. Introduction

Atmospheric aerosols play a crucial role in regulating the Earth's climate through their interactions with solar and terrestrial radiation [1–6]. These minute solid or liquid particles, which originate from both natural and anthropogenic sources such as desert dust, SS, biomass burning, and industrial emissions, have complex effects on the Earth's radiative balance. They can absorb and scatter sunlight, thereby influencing heat distribution in the atmosphere and at the surface [1, 3, 5–8]. The dual nature of aerosols enables them to either warm the atmosphere through absorption or induce cooling by reflecting solar radiation back into space [1, 4, 8, 9].

Aerosols also affect cloud formation [1–4, 9], alter the planetary boundary layer height (PBLH), and influence atmospheric stability, which can have significant implications for weather patterns and long-term climate trends [5, 10]. Additionally, localized heating of the atmosphere by absorbing aerosols, such as black carbon and dust, can exacerbate regional climate ef-

*Corresponding author Tel. No.: +234-803-695-2266.

Email address: tertsea.igbawua@uam.edu.ng (Tertsea Igbawua [ID])

fects, including temperature shifts and changes in precipitation [4, 8, 11].

The impact of aerosols on radiative forcing (RF) has become a critical area of study, particularly for regions like Nigeria, where both natural and anthropogenic aerosols, such as mineral dust from the Sahara and emissions from biomass burning, are prevalent. RF quantifies a shift in the earth's radiation balance owing to perturbation, whether artificial or natural [9]. Radiative heating rates (RHR) on large spatial scales cannot be directly measured and are instead computed using radiative transfer models [12]. Net atmospheric forcing, derived as the difference between TOA and surface forcing, represents the radiative flux absorbed by the atmosphere due to aerosols and is converted into heat as atmospheric heating [11]. AHR is influenced by various factors such as aerosol optical depth (AOD), cloud cover, SSA, and size [5, 7, 8, 12–14]. RHR is a subset of AHR, and while RHR focuses solely on radiative contributions, AHR captures the overall atmospheric temperature dynamics [8, 14].

Previous studies have extensively examined the impact of aerosols on AHR across different regions in Africa and beyond. Liu & Ou [15] reported additional heating of up to 5.5 K/day due to dust absorption in lower atmospheric levels, based on a Sahara dust storm case. In 2006, Satheesh *et al.* [11] found AHR ranging from 0.4 to 1.2 K/day in Southern Africa and from 0.8 to 2.2 K/day in Saudi Arabia. Mallet *et al.* [16] observed significant shortwave (SW) heating within the dusty layer of West Africa (2–4 km), with maximum heating between +4.0 and +7.0 K/day. Lemaître *et al.* [17] found that mineral dust over West Africa caused daytime warming from 1.5 K/day to 4 K/day, with localized areas reaching up to 8 K/day. Pilewskie *et al.* [18] noted RHR exceeding 4 K/day in Mongu, Zambia. In Europe, Kokkalis *et al.* [19] determined a net RHR of +0.156 K/day at the bottom of the atmosphere, increasing to +2.543 K/day within the 1–6 km altitude range. Zhao *et al.* [20] reported an average AHR of 0.8 ± 0.5 K/day in Niamey and 0.5 ± 0.2 K/day over North Africa. Malavelle *et al.* [21] observed a shortwave RHR of 1.2 K/day at local noon over Niamey, while Makokha *et al.* [22] found a net atmospheric forcing of 0.55 ± 0.05 K/day in East Africa's lower troposphere. Meanwhile, Kumar *et al.* [23] reported an atmospheric heating rate of 0.96 K/day in South Africa.

Atmospheric aerosols affect radiative forcing (RF) of the atmosphere through both direct and indirect processes [22]. Directly, they influence the climate by scattering and absorbing shortwave (SW) and longwave (LW) radiation [21]. Indirectly, they impact cloud properties by acting as cloud condensation nuclei (CCN), which help in forming cloud droplets [22]. Aerosol optical properties, such as aerosol optical depth (AOD), Ångström exponent (ANG), single scattering albedo (SSA), volume size distribution, and refractive index, play a vital role in influencing direct aerosol radiative forcing at both the surface (SFC) and the top of the atmosphere (TOA) [23]. Aerosol radiative forcing exhibits significant spatial and temporal variability due to differences in aerosol properties, concentrations, and atmospheric lifespans [24]. These variations influence AHR, which, like most geoscience time series, show seasonal patterns in their records [25]. Understanding these temporal variations and underlying patterns in AHR requires robust analytical tools.

Detrended Fluctuation Analysis (DFA) is a method used to identify patterns in time series data, specifically to detect persistence in data records [26, 27]. DFA helps reveal how persistent these patterns are, and the Hurst exponent, a key result of the DFA method, quantifies this persistence [27]. A Hurst exponent value between 0.5 and 1 indicates persistence, meaning that current conditions are likely to influence future conditions. Conversely, a value below 0.5 suggests short-term changes with minimal lasting effects (anti-persistence) [27].

The influence of atmospheric aerosols on radiative heating, particularly in high aerosol regions such as Nigeria, remains poorly understood despite their significant role in climate dynamics. While numerous studies have quantified the effects of aerosols on AHR in other regions of Africa [11, 16–18, 20–23], there is a critical gap in research focused on Nigeria, a region affected by both natural and anthropogenic aerosol emissions. Aerosols can both warm the atmosphere through absorption and cool it by scattering solar radiation, but their net impact on regional climate patterns, including temperature and precipitation shifts, remains unclear. Understanding these aerosol-induced radiative effects is essential for accurately assessing climate change implications and informing adaptation strategies in Nigeria, where the local climate is increasingly vulnerable to these changes. Therefore, there is an urgent need for focused research on AHR and their influencing factors in Nigeria to address this gap and contribute to regional climate modeling and mitigation efforts. Additionally, the scarcity of in-situ data and the absence of long-term monitoring stations complicate the task of quantifying AHR.

As a result, this work relies on the use of satellite datasets to assess the spatial and temporal aerosol radiative heating over the country. The objectives of this work are to: (1) determine the spatial, annual, and seasonal trends of AHR; (2) assess the factors influencing AHR changes; (3) determine the persistence of AHR; and (4) identify the spatial aerosol type classification in the study area. This approach is vital to address the absence of reliable in-situ data. Additionally, it is crucial for gaining insights into the impact of aerosol emissions on radiative heating in Nigeria.

2. Materials and methods

2.1. Study area

Nigeria, situated in West Africa, shares borders with Benin to the west, Chad and Cameroon to the east, and Niger to the north. Nigeria's topography is varied, featuring expansive savannahs in the north and dense tropical rainforests in the south. The southern region experiences elevated levels of precipitation, humidity, and cloud cover, while the northern regions exhibit lower levels of these climatic variables. Figure 1 shows the study area with the Koppen climate classification system. The Koppen classification codes Af, Am, Aw, BSh, BWh, and
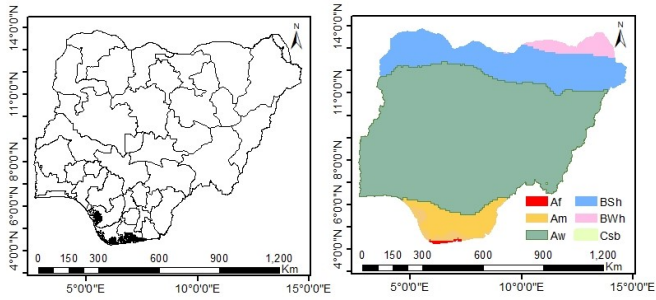
Figure 1: Study area with (a) states and (b) Koppen climate classification.

Csb represent tropical rainforest, tropical monsoon, tropical savanna, hot semi-arid, hot desert, and warm summer Mediterranean climate, respectively [28]. Af, Am, Aw, BSh, BWh, and Csb occupy about 0.23, 6.36, 70.45, 19.73, 3.21 and 0.01%, respectively, of the total land mass of the country. The two basic seasons in Nigeria are the dry and wet seasons. The dry season is marked by a dusty air flow from the Sahara Desert, also known as Harmattan, and the rainy season by a moisture flux from the South Atlantic Ocean [29].

2.2. Data source

The data used in this work is from Modern-Era Retrospective Analysis for Research and Applications, Version 2 (MERRA-2) from the National Aeronautics and Space Administration's (NASA) Global Modeling and Assimilation Office (GMAO). The summary of the data is shown in Table 1 [30–32].

2.3. Methodology
2.3.1. Aerosol radiative heating (AHR) rates over the study area

The AHR for atmospheric heating is given by [8, 14] and was adopted by the study.

$$AHR = \frac{g}{c_p} \frac{ARF_{ATM}}{\Delta P} \left(24\frac{hr}{d} \times 3600\frac{sec}{hr} \right), \quad (1)$$

where g denotes the acceleration due to gravity, c_p represents the specific heat capacity of air at constant pressure (1006 J/kg-K), and ΔP signifies the alteration in atmospheric pressure (in hPa) [14], a height of 5000 meters was selected to encompass the highest elevation point in Nigeria.

$$ARF_{ATM} = ARF_{TOA} - ARF_{SUF}, \quad (2)$$

$$ARF_{TOA} = Net\ Flux_{withaerosolTOA} - Net\ Flux_{withoutaerosolTOA}, \quad (3)$$

$$ARF_{SFC} = [Net\ Flux_{withaerosolSUR} - Net\ Flux_{withoutaerosolSUR}]$$
$$\times (1 - SUAB), \quad (4)$$

where ARF_{ATM}, ARF_{TOA} and ARF_{SUF} represent the atmospheric radiative forcing for the atmosphere, top of the atmosphere, and surface, respectively. The variable $SUAB$ denotes the surface albedo.

2.3.2. Analysis of persistence and prediction of future aerosol trends

The analysis of persistence was employed on the AHR datasets using DFA. This technique, known for its effectiveness in detecting long-term memory in time series, was introduced by Kantelhardt *et al.* [33] as a modification of the method initially described by Peng *et al.* [26]. This analysis was applied to a monthly time series of AHR $\widetilde{\delta}_i$, $i = 1, 2, 3 \ldots N$, then the following methods were adopted:

  i. The seasonal trend is subtracted from the data.
 ii. A profile Q, is created

$$Q(i) = \sum_{k=1}^{i} \widetilde{\delta}_k, i = 1, 2 \ldots, N. \quad (5)$$

iii. The time series was partitioned into N_s equal non-overlapping segments of fixed length s to obtained the fluctuations in Q.
 iv. The ideal polynomial fit $f_l(i)$ of the profile and obtain the variance (Equation (6)) around the fit for each segment $l = 1, 2 \ldots N_s$ was created

$$F_s^2(l) = \frac{1}{s} \sum_{j=1}^{s} [G\left((l-1)s + j\right) - f_l\left((l-1)s + j\right)]^2. \quad (6)$$

  v. The mean of $F_s^2(l)$ over all the segments (N_s) was taken to get the value of the fluctuation function $F(s)$.

The correlation between $F(s)$ and s, as defined in Equation 7, suggests the existence of power-law (fractal) scaling. The parameter h in the equation represents the scaling Hurst exponent. If h is greater than 0.5, the series displays persistence (long-range correlation); if h is less than 0.5, the series exhibits non-persistence (long-range anti-correlation); and when h is equal to 0.5, the series is considered random.

$$F(s) \propto s^h. \quad (7)$$

2.3.3. Single scattering albedo

The Single Scattering Albedo at 550 nm (SSA$_{550}$) was determined as the ratio of scattering efficiency σ_{sca} to extinction efficiency σ_{ext} given by:

$$SSA_\lambda = \frac{\sigma_{sca\lambda}}{\sigma_{ext\lambda}}, \quad (8)$$

where λ is the wavelength. The single scattering albedo values closer to 1 indicate that the medium is more reflective, whereas values closer to 0 indicate that the atmosphere is highly absorbing. The aerosol class type is shown in Table 2 [23, 34, 35].

The aerosol class type technique for determining the class type maps was performed using single scattering albedo (SSA) and Ångström exponent (ANG) data. Based on the established classification scheme (Table 2) [23, 34, 35], aerosols were categorized into different classes: such as coarse-mode, mixed-mode, and fine-mode, depending on the specific values of SSA and ANG. This classification was implemented in ArcMap 10.3.1 using the Reclassify tool, which allowed for the

Table 1: Data sets used in this study (BC=Black carbon, OC=Organic carbon, DU=Dust surface, SS=Sea salt, and SO$_4$=Sulfate) from 2000 to 2022.

SN	Parameter	Resolution	Source
1	BC surface mass conc. (BCSMASS)	0.5×0.625	[30]
2	OC surface mass conc. (OCSMASS)	0.5×0.625	[30]
3	DU surface mass conc. PM25 (DUSMASS25)	0.5×0.625	[30]
4	SO4 surface mass conc. (SO$_4$SMASS)	0.5×0.625	[30]
5	SS surface mass conc. PM25 (SSSMASS25)	0.5×0.625	[30]
6	Surface net downward long wave flux	0.5×0.625	[31]
7	Surface net downward long wave flux assuming clear sky & no aerosol	0.5×0.625	[31]
8	Upwelling long wave flux at TOA	0.5×0.625	[31]
9	Upwelling long wave flux at TOA assuming clear sky & no aerosol	0.5×0.625	[31]
10	Surface net downward flux	0.5×0.625	[31]
11	Surface net downward flux assuming clear sky & no aerosol	0.5×0.625	[31]
12	TOA net downward shortwave flux	0.5×0.625	[31]
13	TOA net downward shortwave flux assuming clear sky & no aerosol	0.5×0.625	[31]
14	Total Aerosol Extinction AOT [550 nm]	0.5×0.625	[31]
15	Total Aerosol Scattering AOT [550 nm]	0.5×0.625	[31]
16	Total Aerosol Angstrom parameter [470-870 nm] (ANG)	0.5×0.625	[31]
17	Aerosol Optical Depth	0.5×0.625	[32]

Table 2: Aerosol type classification based on optical properties.

S/N	SSA	ANG	Aerosol class type
1	$SSA > 0.95$	$ANG \leq 0.6$	Coarse-mode/non-absorbing
2	$SSA \leq 0.95$	$ANG \leq 0.6$	Coarse-mode/absorbing
3	$SSA > 0.95$	$0.6 \leq ANG < 1.2$	Mixed-mode/non-absorbing
4	$SSA \leq 0.95$	$0.6 \leq ANG < 1.2$	Mixed-mode/absorbing
5	$SSA > 0.95$	$ANG > 1.2$	Fine-mode/non-absorbing
6	$SSA \leq 0.85$	$ANG > 1.2$	Fine-mode/highly-absorbing
7	$0.85 \leq SSA < 0.9$	$ANG > 1.2$	Fine-mode/moderately-absorbing
8	$0.9 \leq SSA < 0.95$	$ANG > 1.2$	Fine-mode/slightly-absorbing

segmentation of spatial data into distinct aerosol types. The reclassification process involved setting thresholds for SSA and ANG to define each aerosol class, thereby enabling spatial analysis of aerosol types across the study area.

2.3.4. Transfer entropy (TE) as a tool for causality analysis

The formula for Transfer Entropy (TE) measures the directed information transfer between two time series (M and N), often used to capture the influence of one variable over another in a dynamic system. The basic form of the Transfer Entropy is derived from information theory, specifically from the concept of conditional mutual information [36].

$$TE_{N \to M} = \sum_{m,n} p(m_{t+1}, m_t^{(k)}, n_t^{(l)}) log\left(\frac{p(m_{t+1} | m_t^{(k)}, n_t^{(l)})}{p\left(m_{t+1} | m_t^{(k)}\right)} \right), \quad (9)$$

where $TE_{N \to M}$ is a measure of information flow from n to M, k and l represents their order, m_{t+1} and $m_t^{(k)}$ are the the future and present values of the target variable M, $n_t^{(l)}$ is the present value of the source variable N, $p(m_{t+1}, m_t^{(k)}, n_t^{(l)})$ is the joint

probability distribution of M and N, $p(m_{t+1} | m_t^{(k)}, n_t^{(l)})$ is the conditional probability of m_{t+1} given both $m_t^{(k)}$ and $n_t^{(l)}$, and $p\left(m_{t+1} | m_t^{(k)}\right)$ is the conditional probability of m_{t+1} given only $m_t^{(k)}$.

2.3.5. Mann-Kendall trend test

The Mann-Kendall trend test used in this work is given by [37, 38]:

$$K = \sum_{i=1}^{n-1} \sum_{j=i11}^{n} sgn(y_j - y_i), \quad (10)$$

where n is the number of data points, y_j and y_i are the data values in the time series i and $j(j > 1)$, respectively and $sgn\left(y_j - y_i\right)$ is the sign function given by:

$$sgn\left(y_j - y_i\right) = \begin{cases} +1, & if \ y_j - y_i > 0 \\ 0, & if \ y_j - y_i = 0 \\ -1, & if \ y_j - y_i < 0 \end{cases}. \quad (11)$$

The variance is computed as

$$\text{Var}(K) = \frac{n(n-1)(2n+5) - \sum_{i=1}^{m} t_i(t_i-1)(2t_i+5)}{18}, \quad (12)$$

where n and m are the number of data points and tied groups, and t_i represents the number of ties of extent i. A tied group is a set of sample data with a similar value. In cases where sample
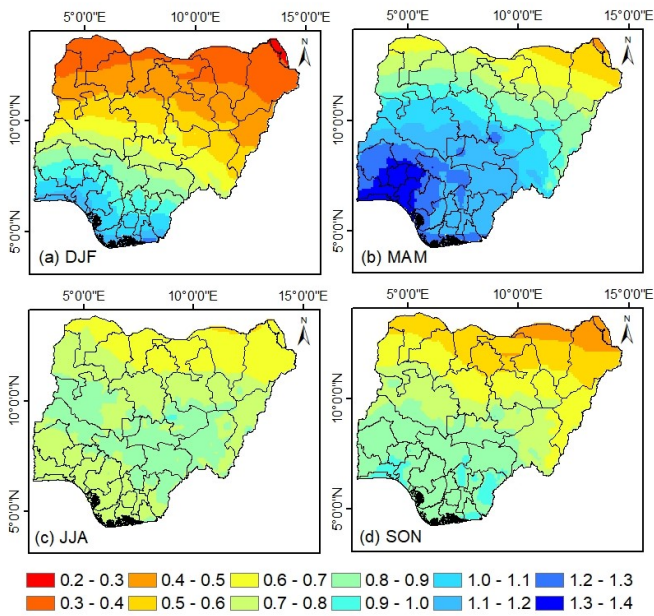
Figure 2: Spatial distribution of AHR across the seasons.

size $n > 10$, the standard normal test statistics M_K is computed as:

$$M_K = \begin{cases} \frac{K-1}{\sqrt{Var(K)}}, & if\ K > 0 \\ 0, & if\ K = 0 \\ \frac{K-1}{\sqrt{Var(K)}}, & if\ K < 0 \end{cases} \quad . \tag{13}$$

A positive (negative) value of M_K indicates an increasing (decreasing) trend. Testing trends is performed at a specific significance level (α). When $|M_K| > M_{1-\alpha/2}$, the null hypothesis is rejected and a significance trend exists in the time series.

3. Results and discussion

3.1. Spatial distribution of AHR over the study area

Figure 2 illustrates the spatial distribution of Atmospheric Heating Rate (AHR) across various seasons in Nigeria from 2000 to 2022. The AHR values were calculated using Equations (1) to (4), representing the net atmospheric forcing caused by aerosols, which is the difference between Top-of-Atmosphere and surface forcing. This forcing leads to heat generation as the energy is transformed into atmospheric warming.

The highest AHR values occur during the MAM (March–April–May) season, followed closely by the DJF season. These peak values are predominantly concentrated along the coastal regions in the southern parts of the study area. In contrast, the JJA and SON seasons exhibit the lowest AHR values, which are primarily scattered near the desert regions. The spatial distribution patterns depicted in Figure 2 showcases the distinct seasonal variations in AHR across the study area.

3.2. Annual and seasonal distribution of AHR

Figure 3 illustrates the annual variation of AHR across climatic zones during various seasons from 2000 to 2022. The

findings reveal that the Af and Am climate zones exhibit notably higher AHR values compared to other zones, while BWh shows the lowest values. Within Af and Am, the MAM and DJF seasons showcase elevated AHR compared to JJA and SON. In Af, DJF and MAM seasons exhibit negative slope changes, while JJA and SON show positive slopes. Similarly, in Aw and Csb, AHR values peak during DJF, with negative slope values for DJF, MAM, and SON, and a positive slope for JJA. In BSh and BWh, high AHR values are observed during MAM and JJA, but BSh exhibits negative slopes across all seasons, while BWh shows negative slopes in DJF and SON and positive slopes in MAM and JJA. The average AHR values in Af, Am, Aw, BWh, BSh, and Csb zones are 1.02±0.02, 0.98±0.03, 0.82±0.11, 0.48±0.01, 0.56±0.03, and 0.86±0.00 K/day, respectively. The annual average for the entire country is 0.77±0.15 K/day, comparable to estimates in East Africa (0.55±0.05 K/day) by Makokha *et al.* [22], South Africa (0.4-1.2 K/day) by Satheesh *et al.* [11], Niamey (0.8±0.5 K/day), and North Africa (0.5±0.2 K/day) by Zhao *et al.* [20].

Figure 4a indicates that the Af region has a positive slope (0.0009), suggesting a slight increase in AHR over time. Conversely, Am shows a minor decline (-0.0005). The Aw zone demonstrates a substantial reduction (-0.0042), while BSh (-0.001) and BWh (-0.0018) reflect decreasing trends. The Csb zone displays a significant negative slope (-0.0035), indicating a notable reduction. Figure 4b highlights high AHR values from January to May and low values from June to October across all zones. The Af and Am zones experience peaks between February and April, while Aw and Csb peak between March and June. BSh and BWh exhibit a bimodal distribution with peaks in April-May and August-September.

Figure 5 shows that high (low) AOD values in the Af and Am zones correspond to high (low) AHR values. During the dry season (November to March), AOD peaks in February and March, coinciding with the Harmattan period when dust aerosols dominate. This period corresponds to higher AHR, indicating the role of absorbing aerosols, such as dust, in increasing AHR. In the rainy season (July to August), lower AOD and AHR values suggest reduced aerosol loads and less atmospheric heating. In BSh and BWh, although AOD levels are lower, higher AHR during March and April highlights the influence of dust aerosols. The consistently lower ANG values in these zones reflect larger aerosols, like dust, which are more prevalent during these months and contribute significantly to AHR. Similarly, the Csb zone, with lower AOD and high SSA, experiences limited heating due to the dominance of scattering aerosols.

The BSh and BWh zones, which are arid and semi-arid, exhibit lower AOD levels compared to the wetter zones. However, the trend of higher AOD and AHR during March and April in these regions suggests the influence of DU aerosols on heating, even at lower concentrations. This is further supported by the ANG, which is consistently lower in these regions, reflecting the presence of larger aerosols such as dust. The low ANG values, especially in March and April, coincide with the highest AHR values, reinforcing the role of dust in enhancing atmospheric heating in arid regions. Similarly, in the CSB zone,
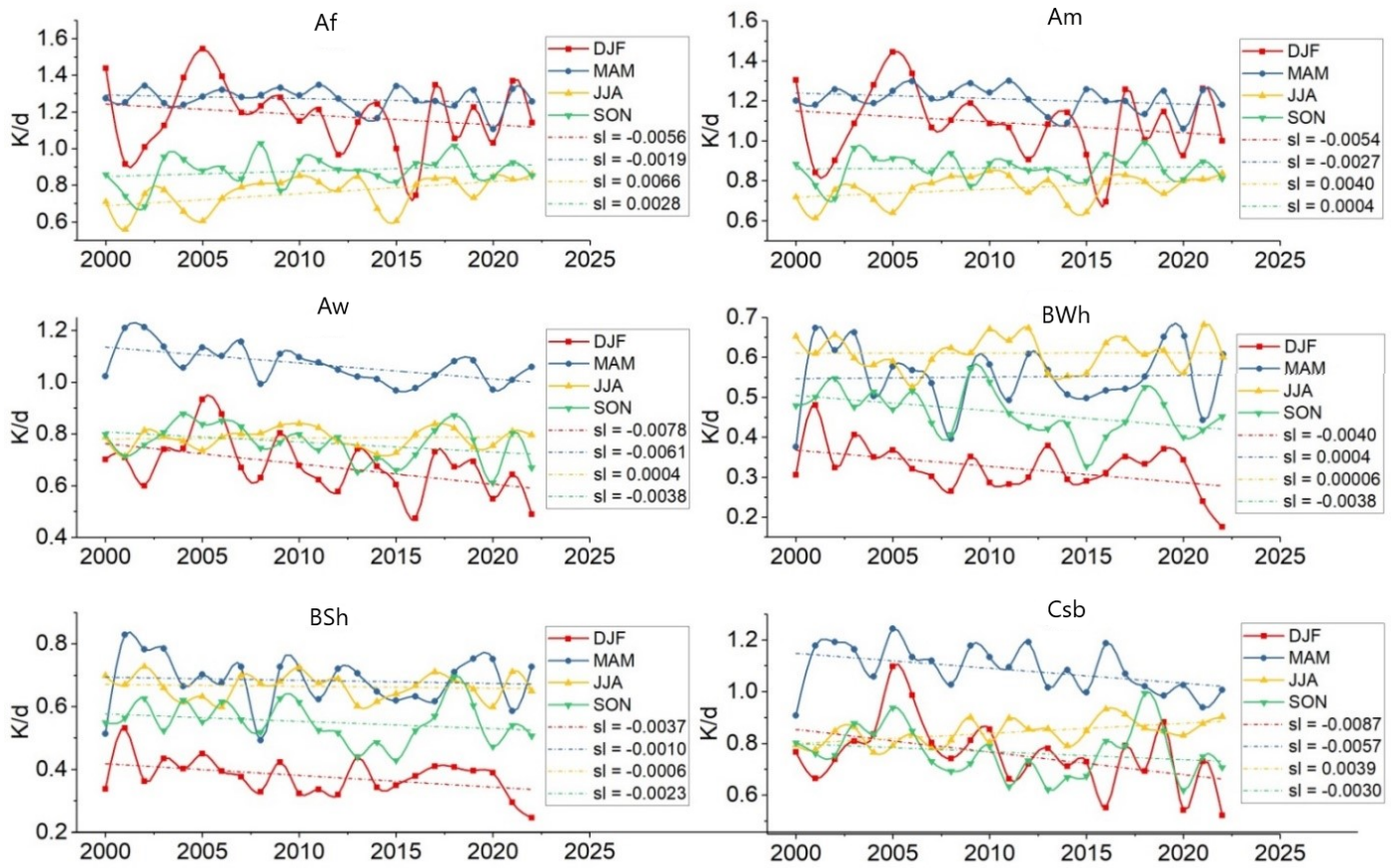
Figure 3: Annual variation of Atmospheric Heating Rate (AHR) across different climatic zones during various seasons.
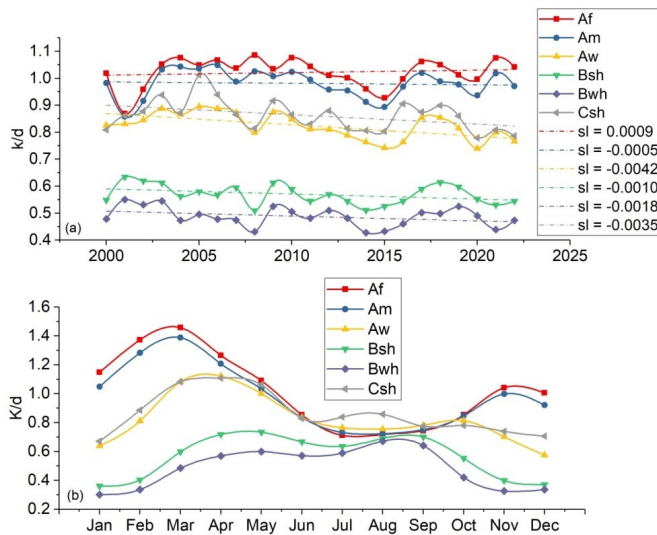

Figure 4: Annual distribution of AHR in different seasons across the different climate systems from 2000 to 2022.

where AOD is lower throughout the year, AHR also remains relatively low, particularly during the rainy season when aerosol content is minimal (Figure 5).

In Af, Am, and Aw, SSA values above 0.90 indicate scat-tering aerosols [34], typically reducing AHR. However, during the dry season, AHR remains elevated, likely due to absorbing aerosols such as dust and biomass-burning products. In BSh and BWh, lower SSA values, especially in March and April, correspond to the absorbing nature of dust aerosols, enhancing AHR. In the Csb zone, high SSA values and low AOD result in minimal heating.

Seasonal changes in OC and BC concentrations across Nigeria are significantly influenced by anthropogenic activi-ties and wet deposition. In Af, Am, and Aw, biomass burn-ing elevates BC, contributing to radiative heating, especially in coastal states where gas flaring in the Niger Delta further am-plifies BC's impact. Conversely, OC aerosols scatter solar ra-diation, cooling the atmosphere, although their interaction with BC complicates their net effect. In BSh and BWh, DU aerosols play a dual role, scattering sunlight and absorbing longwave ra-diation. Seasonal peaks in DU (November to February) and SU reflect the interplay of regional dynamics, corroborating find-ings by Balarabe *et al.* [39]. Additionally, SS aerosols from oceans contribute to cooling in coastal zones, offsetting warm-ing from other aerosols.

3.3. Persistence of AHR in Nigeria

The analysis of persistence and long-range correlation was done using Equations (5) to (7). Figure 6 illustrates the spa-
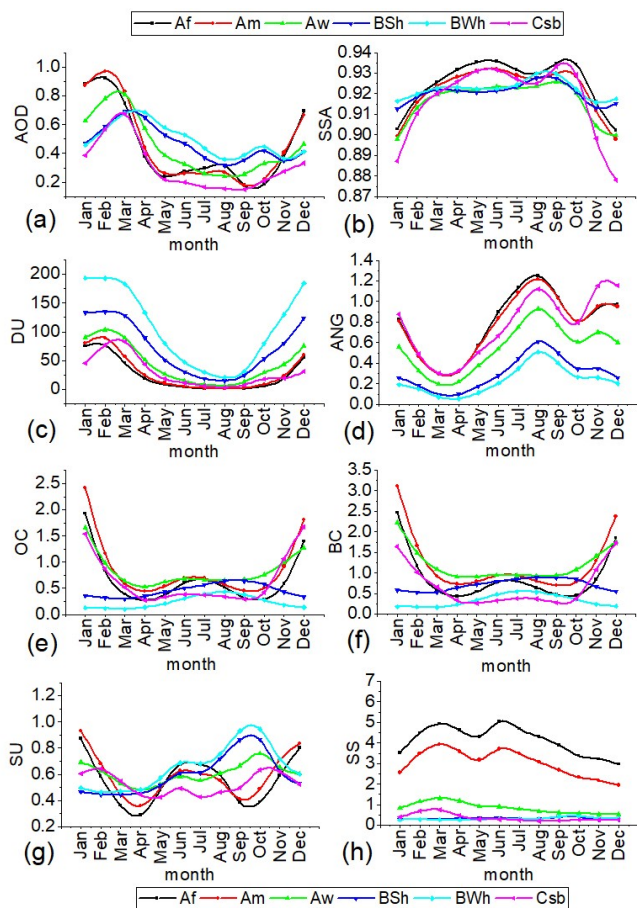
Figure 5: Monthly distributions of AOD, SSA, ANG, DU, OC, BC, SU, and SS from 2000 to 2022.
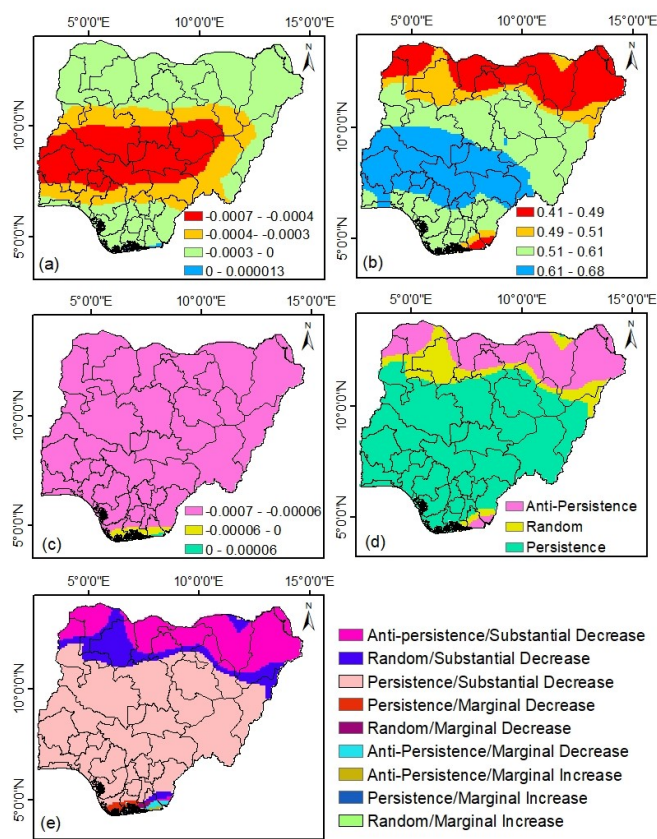

Figure 6: Spatial distribution of AHR from 2000 to 2022. (a) the Linear Regression of AHR, (b) the Hurst exponent, (c) reclassified AHR map depicting low, mid, and high slope values, (d) reclassified map of AHR Hurst exponent, with $H < 0.5$, $H = 0.5$, and $H > 0.5$, and (e) superimposed map combining slope and Hurst exponent.

tial distribution of key parameters related to AHR from 2000 to 2022. The subfigures include (a) linear regression of AHR, (b) distribution of Hurst exponent, (c) a reclassified AHR map depicting low, mid, and high slope values, (d) a reclassified map of AHR Hurst exponent categorizing values with $h < 0.5$, $h = 0.5$, and $h > 0.5$, and finally, (e) a superimposed map combining slope and Hurst exponent information. The results reveal that areas with persistence/substantial decrease (P/SD) in AHR values constituted 66.34%, followed by anti-persistence/substantial decrease (AP/SD) with 21.25% and random/substantial decrease (R/SD) with 10.77%. The highest range of AHR values occurred during the DJF and MAM seasons. AHR values indicating persistence/marginal increase (P/MI) and random/marginal increase (R/MI) had the lowest percentages, with 0.08% and 0.09%, respectively.

The observed persistence in AHR values suggests a correlation between observations at different time points, indicating a tendency to follow a pattern over an extended period. This finding highlights that AHR values in Nigeria have exhibited persistence, fluctuations, or randomness across different regions of the country. Table 3 provides the ranges of AHR values in various seasons, corresponding to slope and Hurst values. These results suggest that AHR, akin to other physical quantities, pos-

sesses fractal qualities, causing its values to persist, revert to the mean, or fluctuate randomly in the future based on factors influencing it. Generally, areas with both low and high AHR values exhibit persistence. Specifically, regions with substantial decreases in AHR have higher DU compared to those with marginal decreases and increases. In contrast, TCC and SS are lower in areas with substantial decreases in AHR but higher in areas with marginal decreases and increases. Aerosol components like OC, BC, and SU originating from natural and anthropogenic activities exhibited variability across all AHR change zones.

Spatial maps indicated that areas exhibiting persistence, randomness, and anti-persistence properties constitute 67.2%, 11.1%, and 21.7%, respectively (Figure 6). persistence areas are observed in the southwest, southeast, north-central, parts of the south-south, and parts of the northeast and northwest. Conversely, regions showing randomness and anti-persistence are located predominantly in the core north and small areas in the south-south zone of Nigeria (Figure 6). The persistence of AHR in Nigeria is detailed in Figure 6, which presents key parameters related to atmospheric warming. The spatial distribu-

Table 3: Comparison between AHR change trends, Hurst exponent and mean AHR values for each class type. TCC ranges from 1 to 0, and Comp. (%) represents the percentage composition of each class type.

AHR change type	Comp. %	Hurst	AHR K/day	BC μgm^{-3}	OC μgm^{-3}	DU μgm^{-3}	SU μgm^{-3}	SS μgm^{-3}	TCC
Anti-persistence/ Substantial Decrease	21.25	0.46	0.72	0.67	4.34	74.76	0.61	0.32	0.47
Random/ Substantial Decrease	10.77	0.50	0.74	0.91	5.97	58.18	0.58	0.44	0.52
persistence/ Substantial Decrease	66.34	0.60	0.80	1.25	8.74	42.30	0.61	1.00	0.68
persistence/ Marginal Decrease	0.79	0.53	1.00	1.12	7.84	26.70	0.57	3.59	0.82
Random/ Marginal Decrease	0.24	0.50	1.02	1.17	8.29	27.83	0.64	3.50	0.83
Anti-persistence/ Marginal Decrease	0.34	0.48	1.03	0.96	7.28	28.63	0.65	3.33	0.84
Anti-persistence/ Marginal Increase	0.10	0.48	1.06	0.90	6.79	27.43	0.65	3.74	0.83
persistence/ Marginal Increase	0.08	0.52	1.03	1.11	7.55	25.56	0.57	4.18	0.81
Random/ Marginal Increase	0.09	0.50	1.05	1.08	7.53	25.78	0.59	4.24	0.81

tion reveals that areas with persistence and substantial/decrease in AHR values constitute the majority (66.34%), followed by anti-persistence/substantial decrease (21.25%), and Random/substantial decrease (10.77%). The persistence in AHR values suggests a correlation between observations at different time points, indicating a tendency for AHR to follow a pattern over an extended period. The analysis highlights the fractal qualities of AHR, as seen in Table 3, suggesting its values persist, revert to the mean, or fluctuate randomly in the future based on factors influencing AHR. Regions with a marginal increase in AHR (regardless of persistence or randomness) exhibited lower values of DU, while higher values were observed for SS, compared to regions with substantial decreases in AHR (regardless of persistence or randomness). However, BC, OC, and SU showed variations in mean values across AHR change zones (Table 3). The spatial maps of BC, OC, DU, SU, and SS are shown in Figure 7.

Figure 8 shows the range of values for (a) AHR, (b) AOD, (c) ANG, (d) SSA, (e) BC, (f) DU, (g) OC, (h) SU, and (i) SS across various AHR regions. The results indicate that areas with substantially decreased AHR, AOD, SSA, ANG, BC, OC, and SS exhibit lower mean AHR values and a narrower range compared to areas with marginal decreases or increases (Tables 3 and 4). Lower mean values in the AP/SD, R/SD, and P/SD regions indicate the presence of larger aerosol particle sizes [40, 41]. The mean values for AHR, AOD, SSA, BC, OC, SU, and SS in the AP/SD and R/SD regions are the lowest compared to DU. In contrast, DU shows a higher mean and a wider range of values in the AP/SD and R/SD regions compared to other areas (Table 3 and Figure 8).

Spatial DFA analysis was used to identify areas with persistence and random behavior, while increasing or decreasing trends in AHR were determined using a linear regression model. The DFA and OLR were combined in ArcMap 10.3.1 to produce a composite map, labeling regions as persistence, anti-persistence, or random with increasing or decreasing trends. The Mann-Kendall trend test was used to determine the trends of the AHR, AOD, SSA, ANG, BC, OC, DU, SU, and SS variables.

The regions characterized by anti-persistence/substantial decreases (AP/SD), random/substantial decreases (R/SD), and persistence/substantial decreases (P/SD) in AHR show a dominant influence of scattering aerosols, which lead to atmospheric cooling despite the presence of absorbing aerosols like BC. In AP/SD regions, the decrease in AHR, despite a significant increase in BC, indicates that the cooling effect of scattering aerosols such as OC, SU, and SS outweighs the warming contribution of BC. Similarly, R/SD regions exhibit only a minor decrease in AHR, with fluctuations driven by competing aerosol effects, where the cooling influence of OC, SU, and SS counteracts the warming from BC. In P/SD regions, the persistence decline in AHR is again attributed to the dominance of scattering aerosols, despite a decrease in SSA and an increase in BC. In general, the cooling effects of scattering aerosols consistently outweigh the warming influence of absorbing aerosols in these regions (Table 4).

In areas where atmospheric heating rates (AHR) show persistence/marginal decreases (P/MD), random/marginal decreases (R/MD), and anti-persistence/marginal decreases (AP/MD), the interplay between absorbing and scattering aerosols leads to slight but steady reductions in heating. P/MD regions show stable aerosol concentrations, as indicated by insignificant changes in AOD, while a significant decrease in SSA reflects a shift toward more absorbing aerosols [14, 40]. The increase in OC and the stable presence of SU and SS result in marginal decreases in AHR, where cooling effects offset warming.

In R/MD regions, marginal decreases in AHR occur due to a balance between rising BC levels and reductions in SSA and SU. This combination creates random fluctuations that ultimately lead to slight cooling trends. Similarly, in AP/MD regions, short-term increases in BC-driven heating are offset by decreases caused by scattering aerosols like SU, resulting in small but fluctuating declines in AHR. These patterns highlight how shifts in aerosol characteristics, especially the interplay between absorbing and scattering aerosols play a key role in influencing slight changes in AHR.

Regions with anti-persistence/marginal increases (AP/MI), persistence/marginal increases (P/MI), and random/marginal increases (R/MI) in AHR highlight the influence of absorbing aerosols like BC. In AP/MI regions, significant increases in BC and decreases in SSA indicate a dominance of absorbing
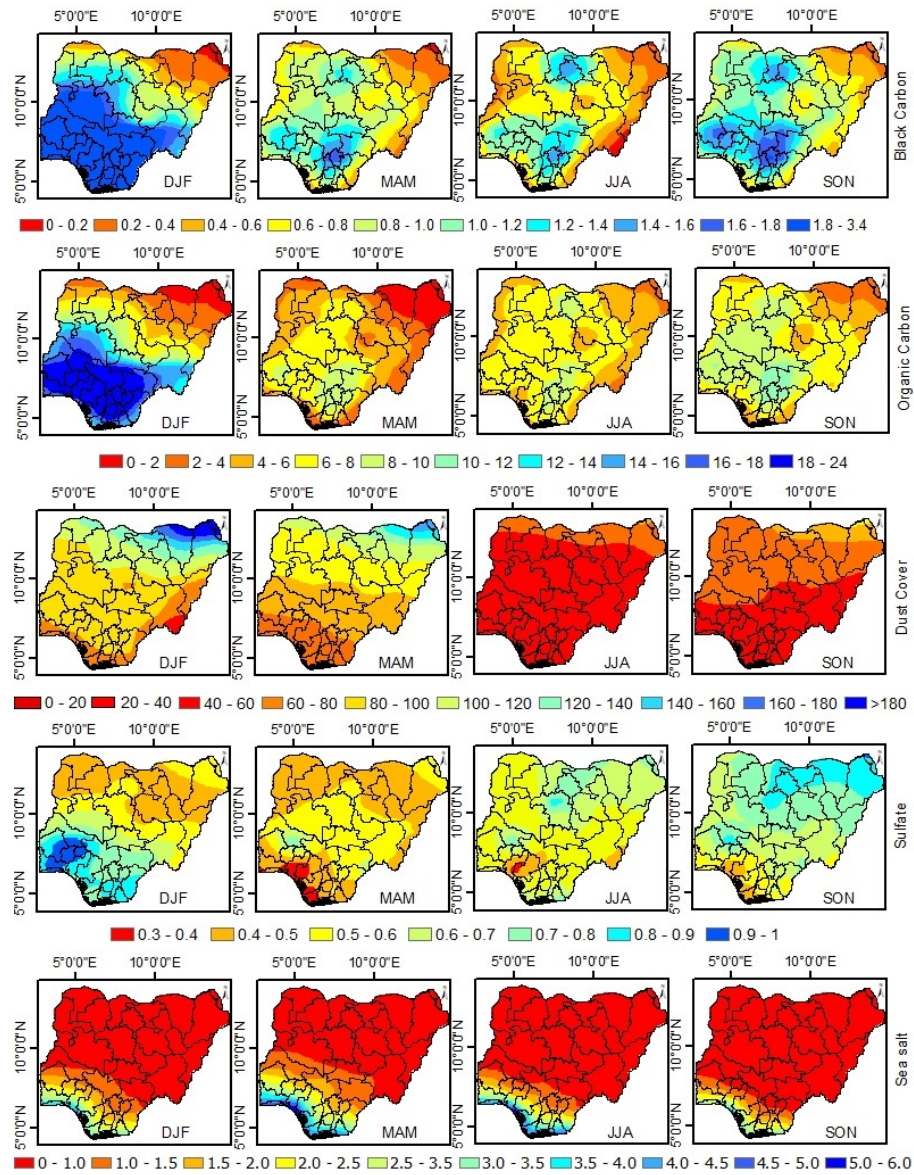
Figure 7: Spatial distributions of aerosol parameters (BC, OC, DU, SU, and SS) in DJF, MAM, JJA and SON from 2000 to 2022.

Table 4: Mann Kendall trend test for the variables in the AHR change regions (Significant codes: 0.1(*), 0.05(**), 0.001(***), and 0.0000(****)).

Variable/ AHR Change type	AHR	AOD	SSA	ANG	BC	DU	OC	SU	SS
Anti-persistence/ Substantial Decrease	-0.054	-0.019	-0.064	0.048	0.159***	-0.017	0.119**	0.041	0.055
Random/ Substantial Decrease	-0.047	-0.006	-0.056	0.027	0.205****	0.000	0.123**	0.041	0.057
persistence/ Substantial Decrease	-0.098**	-0.009	-0.120***	-0.011	0.107**	0.014	0.078*	-0.018	-0.030
persistence/ Marginal Decrease	-0.003	-0.017	-0.206***	-0.026	0.095**	0.014	0.056	-0.069	-0.027
Random/ Marginal Decrease	-0.003	-0.014	-0.211****	-0.030	0.103**	0.016	0.060	-0.081**	-0.039
Anti-persistence/ Marginal Decrease	-0.001	-0.015	-0.205****	-0.035	0.073*	0.018	0.040	-0.087**	-0.039
Anti-persistence/ Marginal Increase	0.005	-0.015	-0.201****	-0.034	0.064*	0.016	0.038	-0.088**	-0.025
persistence/ Marginal Increase	0.000	-0.018	-0.202****	-0.026	0.096**	0.013	0.060	-0.074*	-0.030
Random/ Marginal Increase	0.003	-0.017	-0.204****	-0.029	0.093**	0.014	0.060	-0.074*	-0.030

aerosols [14, 40], which enhance atmospheric heating. Similarly, P/MI regions exhibit a stable aerosol load but a shift toward absorbing aerosols, as evidenced by increases in BC and

decreases in SSA. Reduced cooling from SU further contributes to these heating trends. In R/MI regions, random fluctuations in AHR arise from the interplay between increased BC absorption
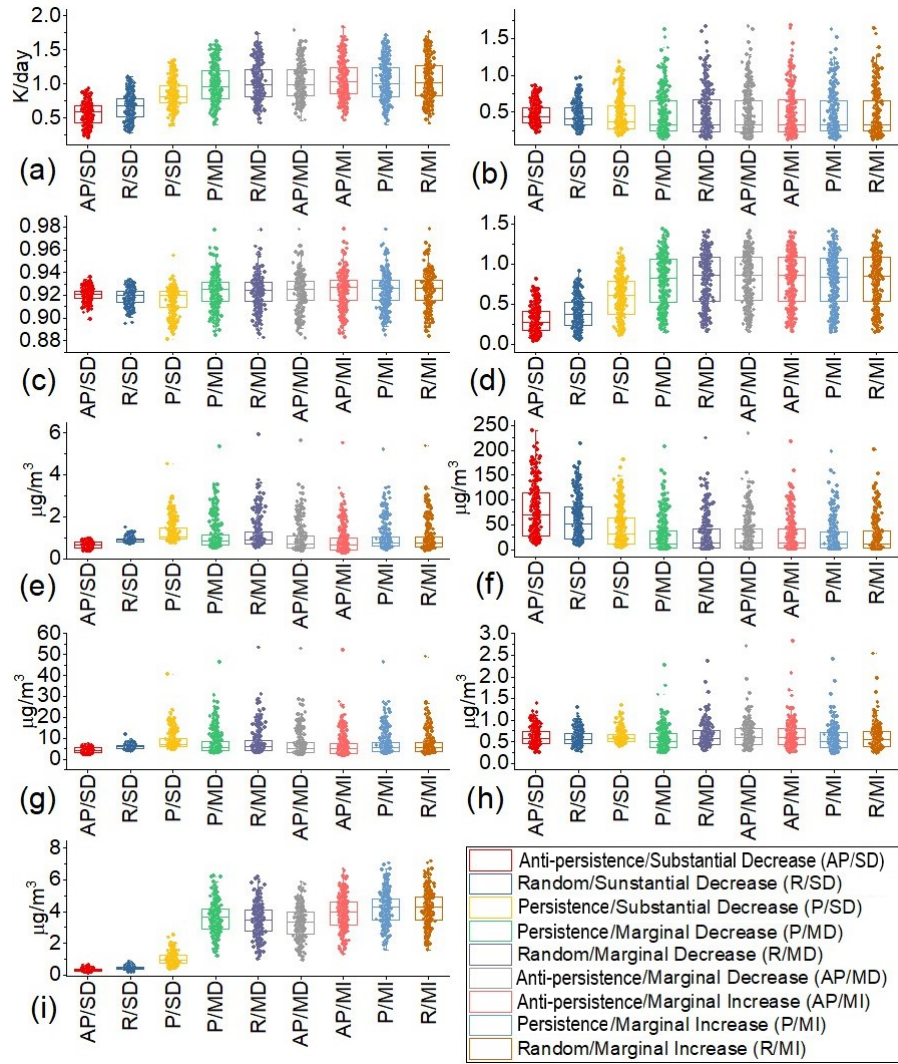
Figure 8: Range of values for (a) AHR, (b) AOD, (c) ANG, (d) SSA, (e) BC, (f) DU, (g) OC, (h) SU, and (i) SS across various AHR regions.

Table 5: Normalized Information Flow (NIF) between AHR and aerosol optical properties, climate and aerosol variables (Significant codes: 0.1(*), 0.05(**), 0.001(***), and 0.0000(****)).

Variable/ AHR Change type	AOD	SSA	ANG	BC	DU	OC	SU	SS
Anti-persistence/ Substantial Decrease	0.0231	0.019	0.041*	0.028	0.018	0.025	0.010	0.010
Random/ Substantial Decrease	0.006	0.013	0.023	0.018	0.014	0.022	0.010	0.010
persistence/ Substantial Decrease	0.080**	0.003	0.015	0.022	0.011	0.072	0.041	0.155
persistence/ Marginal Decrease	0.059	0.050*	0.009	0.074	0.179****	0.096	0.054	0.037
Random/ Marginal Decrease	0.062**	0.051	0.010	0.054	0.040****	0.110**	0.078	0.012
Anti-persistence/ Marginal Decrease	0.055	0.026	0.030	0.015	0.112****	0.022	0.103	0.055*
Anti-persistence/ Marginal Increase	0.070*	0.026	0.024	0.030	0.070**	0.025	0.037*	0.039
persistence/ Marginal Increase	0.023	0.052**	0.015	0.060	0.141*	0.048	0.029	0.027
Random/ Marginal Increase	0.043	0.056*	0.013	0.042*	0.056****	0.038	0.028	0.034

and diminished SU cooling. These overall trends reflect the predominance of absorbing aerosols, driving marginal increases in AHR (Table 4). Collaud *et al.* [42] attributed decreasing BC trends to traffic-related emissions rather than industrial or biomass-burning sources.

Our findings show that AHR exhibits an inverse relationship with SSA [8, 14, 40]. As SSA decreases, indicating a dominance of absorbing aerosols such as BC, AHR increases due to enhanced atmospheric heating. Conversely, higher SSA, associated with scattering aerosols, reduces AHR [8, 14, 40]. The
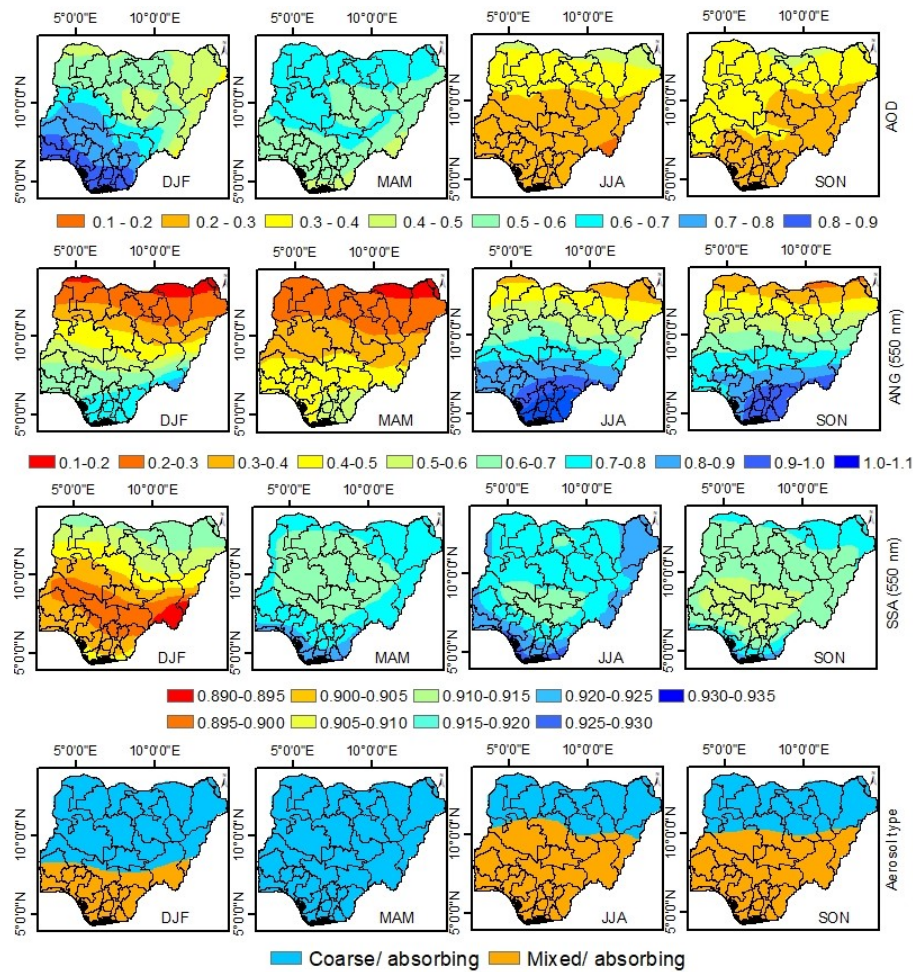
Figure 9: Spatial distribution of seasonal Aerosol optical depth (AOD), Angstrom parameter 470-870 nm (ANG), Single scattering albedo 550nm (SSA$_{550}$), and Aerosol distribution type from 2000 to 2022.

relationship between AHR and AOD is generally positive, as increased AOD reflects higher aerosol concentrations, often leading to more atmospheric heating when absorbing aerosols dominate. However, the effect diminishes when scattering aerosols prevail. Kumar *et al.* [23] and Srivastava *et al.* [43] noted that AOD influences SSA, with higher AOD correlating with lower SSA due to increased aerosol absorption.

Specific aerosol types display diverse impacts. DU aerosols exhibit a cooling effect, contributing to a minor inverse relationship with AHR in some regions. BC, with its strong absorptive properties, consistently increases AHR [40], while OC, SS, and SU, primarily scattering aerosols, promote atmospheric cooling. Guleria and Kuniyal [44] observed a strong atmospheric forcing response during dust-laden periods, while Gómez-Amo *et al.* [45] highlighted how DU within atmospheric layers affects AHR.

The relationships among SSA, AOD, and ANG further illuminate these dynamics. SSA negatively correlates with AOD [40, 41, 46], as higher AOD suggests more absorbing aerosols, lowering SSA. AOD also positively correlates with ANG, as smaller fine-mode aerosols associated with higher ANG values are efficient at absorbing radiation. ANG and SSA exhibit a negative relationship [40, 41], with higher ANG values, indicative of smaller particles, correlating with lower SSA and a greater presence of absorbing aerosols [47]. High ANG values reflect the influence of aerosols from biomass burning, vehicular emissions, or secondary gas-formed aerosols [48–50]. AHR positively correlates with ANG, as smaller, more absorbing aerosols enhance atmospheric heating [40, 41].

The interactions between SSA, AOD, and solar radiation play a key role in shaping atmospheric heating. While scattering aerosols generally have a cooling effect [14, 47], predicting AHR becomes more complex in regions with diverse aerosol mixtures [23, 43]. Other atmospheric and meteorological factors, such as clouds, planetary boundary layer height (PBLH), and sea surface temperature (SST), also modulate heating. Raj *et al.* [51] emphasized the role of PBLH in influencing aerosol properties, while Zou *et al.* [52] demonstrated that PBLH decreases more rapidly with increasing aerosol loads. Wang *et al.* [53] identified correlations between atmospheric radiative forcing and PBLH, while Roberts *et al.* [54] and Wang *et al.* [55] linked seasonal SST warming in the Atlantic Ocean to higher AHR during MAM.

3.4. Detecting causal relationships between ahr and aerosol optical and concentration variables

Table 5 presents the results of the normalized information flow (NIF) analysis used to determine the influence of optical and aerosol variables on AHR across different AHR change zones. In the AP/SD and R/SD zones, ANG had the highest influence on AHR, with values of 0.041 and 0.023, respectively, while other variables, particularly SU and SS, showed minimal influence with values of 0.010 in both zones. In the P/SD zone, SS exhibited the highest influence on AHR (0.155), whereas SSA had the lowest impact, with an insignificant value of 0.003.

For zones with a persistence marginal decrease (P/MD) in AHR, DU (0.179) was identified as the primary influencing variable, followed by SSA (0.050). SS and OC also exhibited notable connections with AHR. In contrast, in the R/MD zones, the primary influences on AHR were OC (0.110), AOD (0.062), and DU (0.040), while the remaining variables exhibited lower impacts. In the AP/MD zones, DU (0.112) and SS (0.055) emerged as the most influential variables affecting AHR changes. In the AP/MI zones, AOD (0.070), DU (0.070), and SU (0.037) demonstrated significant contributions to AHR variability. For the P/MI zones, SS (0.052) and DU (0.141) were identified as the dominant variables. In the R/MI zones, SSA (0.056), DU (0.056), and BC (0.042) exhibited significant influence on AHR.

3.5. Spatial distribution of aerosol type classification based on optical properties

Figure 9 presents the spatial distribution of AOD, ANG, SSA_{550}, and aerosol type classification across the seasons. High AOD values were prevalent during the DJF season, followed by MAM, then JJA and SON. Conversely, higher ANG values were observed in JJA and SON compared to DJF and MAM. SSA550 values were higher in MAM and JJA, followed by SON and DJF. The AOD values ranged from 0.37 to 0.87 (DJF), 0.40 to 0.67 (MAM), 0.16 to 0.49 (JJA), and 0.20 to 0.44 (SON). ANG values ranged from 0.16 to 0.91 (DJF), 0.07 to 0.43 (MAM), 0.30 to 1.08 (JJA), and 0.27 to 1.02 (SON). SSA550 values ranged from 0.89 to 0.92 (DJF), 0.92 to 0.93 (MAM), 0.92 to 0.93 (JJA), and 0.91 to 0.93 (SON).

The classification of aerosol types showed that in DJF, 72.1% of aerosols were coarse/absorbing, and 27.9% were mixed/absorbing. In MAM, 100% of aerosols were mixed/absorbing. In JJA, 41.1% were coarse/absorbing, and 58.9% were mixed/absorbing. Similarly, in SON, 44.2% were coarse/absorbing, and 55.8% were mixed/absorbing.

During JJA and SON, the annual mean SSA values (0.92 and 0.91) and ANG values (0.76 and 0.70) indicate a dominance of scattering over absorption by smaller aerosols compared to DJF and MAM. This pattern contributes to moderate atmospheric heating, influenced by increased wind circulation, lower temperatures, and higher cloud cover. The absence of low-level clouds impacts the earth's energy balance by permitting more radiation to reflect back into the atmosphere [7, 13]. SSA values in this work corroborate those obtained by Aladodo *et al.* [35] in Nigeria at Ilorin.

Figures 2 and 7 demonstrate higher AHR and AOD values during the dry season compared to the rainy season, particularly in southern regions. This suggests a significant release of coarse/absorbing aerosols from agricultural activities, dust storms, urban and industrial emissions, biomass burning, and vehicular emissions in northern Nigeria. In southern Nigeria, mixed and absorbing aerosols are predominantly released from urban and industrial emissions, biomass burning [35], marine emissions, gas flaring, and vehicular exhaust. Urban centers likely emit higher aerosol concentrations than rural areas, correlating with regions experiencing elevated AHR values.

Seasonal and annual AOD patterns align with AHR variations, as previously reported by Perrone *et al.* [56]. The study indicates that aerosol absorption by coarse-mode aerosols dominates in northern Nigeria, while mixed-mode aerosols prevail in southern Nigeria during DJF, JJA, and SON. ANG and SSA_{550} values suggest relatively weak aerosol absorption across all seasons except during the dry season. SSA values below 0.89, as highlighted by Khamala *et al.* [34], signify atmospheric warming, while values near 1 indicate significant scattering.

Khamala *et al.* [34] characterized absorbing aerosols as fine and coarse-mode, with dominance varying by location. For example, Mbita showed a predominance of absorbing aerosols using SSA440. Additionally, Kumar *et al.* [23] found that low SSA440 values in SON (0.84) in South Africa were attributed to fine-mode absorbing aerosols from biomass burning.

4. Conclusion

The study examined the spatial and temporal patterns of AHR throughout different seasons in Nigeria from 2000 to 2022, employing a radiative transfer model. The analysis included the assessment of AHR persistence and causal analysis between AHR and influencing variables, and Mann-Kendall trend test. The average AHR for the country was determined to be 0.77±0.15 K/day, with higher values predominantly concentrated in the southern regions compared to the north. In AP/SD and R/SD, ANG had the highest influence on AHR, with TE values of 0.041 and 0.023, respectively, suggesting the influence of fine-mode aerosols. In P/SD and P/MD, SS (0.155) and DU (0.179), respectively, emerged as the dominant influencing variables on AHR. For R/MD and AP/MD, OC (0.110) and DU (0.112) stood out as the relevant variables influencing AHR.

Typically, low (high) AOD, AHR, OC, and BC values corresponded with high (low) SSA values. Aerosol absorption occurs only when SSA values drop below 0.89, which is observed solely in the Csb zone from November to February. In other zones, mean SSA values exceeded 0.89, indicating scattering as the dominant process. This implies reduced (increased) aerosol absorption between March and October (November to February), suggests that the atmosphere scatters more energy than it absorbs, leading to limited heating, especially during the rainy season. This is attributed to the distribution of absorbing aerosols (BC) and scattering aerosols (OC, SU, SS, and dust) in Nigeria, with scattering predominating absorption.

The use of DFA to examine the persistence of AHR reveals that areas with P/SD in AHR values constitute the majority (66.34%). Areas exhibiting AP/SD and those showing R/SD make up 21.25% and 10.77%, respectively. In addition, the study's result explains interactions between various aerosol properties and AHR across different regions and trends. In areas with significant decreases in AHR, such as AP/SD, R/SD, and P/SD, scattering aerosols like OC, SU, and SS dominated, leading to net cooling effects despite the presence of absorbing aerosols like BC. In contrast, regions with persistence and random marginal decreases (P/MD, R/MD, and AP/MD) exhibited a complex balance between absorbing and scattering aerosols, resulting in marginal decreases in AHR. This balance reflects the nuanced role of aerosol types in influencing atmospheric dynamics, with larger particle sizes associated with DU and SS playing a pivotal role in cooling, particularly in regions where these aerosol types were prevalent.

In regions exhibiting marginal increases in AHR, both persistence (P/MI) and random (R/MI), absorbing aerosols such as BC became more influential, contributing to slight increases in atmospheric heating. The decrease in SSA, indicative of more absorbing aerosols, further emphasizes the contribution of BC and other fine-mode aerosols to heating in these regions.

The results of this research are essential for improving our understanding of AHR and the resulting implications for Nigeria's climate plan of action. Through an understanding of the temporal and spatial patterns of atmospheric heating rates (AHR) and their correlation with different forms of aerosol, this study offers essential insight into the ways in which aerosol composition impacts regional climate dynamics. The results underline the importance for informed climate plans that include the intricate interplay between aerosols and atmospheric processes. This investigation provides relevant information that can help policymakers create efficient adaptation and mitigation plans to address the effects of aerosols on the environment and public health as Nigeria struggles with the effects of climate change.

Data availability

The data used in this study is sourced from the Modern-Era Retrospective Analysis for Research and Applications, Version 2 (MERRA-2), provided by the National Aeronautics and Space Administration's (NASA) Global Modeling and Assimilation Office (GMAO). The datasets are publicly available and can be accessed via the following DOIs: https://doi.org/10.5067/FH9A0MLJPC7N, https://doi.org/10.5067/OU3HJDS973O0, and https://doi.org/10.5067/XOGNBQEPLUC5.

References

[1] M. O. Andreae, "Climatic effects of changing atmospheric aerosol levels", in *World survey of climatology* , A. Henderson-Sellers (Ed.), Elsevier B.V., Amsterdam, Netherlands, 1995, pp. 347–398. https://doi.org/10.1016/S0168-6321(06)80033-7.

[2] K. Peters, J. Quaas & N. Bellouin, "Effects of absorbing aerosols in cloudy skies: a satellite study over the Atlantic Ocean", Atmospheric Chemistry and Physics **11** (2011) 1393. https://doi.org/10.5194/acp-11-1393-2011.

[3] S. Liu, J. Xing, B. Zhao, J. Wang, S. Wang, X. Zhang & A. Ding, "Understanding of aerosol–climate interactions in China: aerosol impacts on solar radiation, temperature, cloud, and precipitation and its changes under future climate and emission scenarios", Current Pollution Reports **5** (2019) 36. https://doi.org/10.1007/s40726-019-00107-6.

[4] X. Ling and X. Han, "Aerosol impacts on meteorological elements and surface energy budget over an urban cluster region in the Yangtze River Delta", Aerosol and Air Quality Research **5** (2019) 1040. https://doi.org/10.4209/aaqr.2017.12.0602.

[5] S. P. Cochrane, K. S. Schmidt, H. Chen, P. Pilewskie, S. Kittelman, J. Redemann, S. LeBlanc, K. Pistone, M. Segal Rozenhaimer, M. Kacenelenbogen, Y. Shinozuka, C. Flynn, R. Ferrare, S. Burton, C. Hostetler, M. Mallet & P. Zuidema, "Biomass burning aerosol heating rates from the ORACLES (ObseRvations of Aerosols above CLouds and their intEractionS) 2016 and 2017 experiments", Atmospheric Measurement Techniques **15** (2022) 61. https://doi.org/10.5194/amt-15-61-2022.

[6] K. S. Carslaw, "Aerosol in the climate system", in *Aerosol and Climate*, K. S. Carslaw (Ed.), Elsevier, Amsterdam, Netherlands, 2022, pp. 9–52. https://doi.org/10.1016/C2019-0-00121-5.

[7] G. Cesana, D. E. Waliser, D. Henderson, T. S. L'Ecuyer, X. Jiang & J.-L. F. Li, "The vertical structure of radiative heating rates: a multimodel evaluation using a-train satellite observations", Journal of Climate **32** (2019) 1573. https://doi.org/10.1175/JCLI-D-17-0136.1

[8] Q. Lu, C. Liu, D. Zhao, C. Zeng, J. Li, C. Lu, J. Wang & B. Zhu, "Atmospheric heating rate due to black carbon aerosols: uncertainties and impact factors", Atmospheric Research **240** (2020) 104891. https://doi.org/10.1016/j.atmosres.2020.104891

[9] G. Myhre, C. E. L. Myhre, B. H. Samset & T. Storelvmo, "Aerosols and their relation to global climate and climate sensitivity", Nature Education Knowledge **4** (2013) 7. https://www.researchgate.net/profile/Cathrine-Lund-Myhre/publication/259117107_Aerosols_and_their_Relation_to_Global_Climate_and_Climate_Sensitivity/links/557ecb1208ae26eada8f4606/Aerosols-and-their-Relation-to-Global-Climate-and-Climate-Sensitivity.pdf.

[10] J. Zou, J. Sun, A. Ding, M. Wang, W. Guo & C. Fu, "Observation-based Estimation of Aerosol-induced Reduction of Planetary Boundary Layer Height", Advances in Atmospheric Sciences **34** (2017) 1057. https://doi.org/10.1007/s00376-016-6259-8.

[11] S. K. Satheesh, S. Deepshikha & J. Srinivasan, "Impact of dust aerosols on Earth-atmosphere clear-sky albedo and its short wave radiative forcing over African and Arabian regions", International Journal of Remote Sensing **27** (2006) 1691. https://doi.org/10.1080/01431160500462162.

[12] S. Kato, F. G. Rose, S. H. Ham, D. A. Rutan, A. Radkevich, T. E. Caldwell, S. Sun-mack, W. F. Miller & Y. Chen, "Radiative heating rates computed with clouds derived from satellite-based passive and active sensors and their effects on generation of available potential energy", J. Geophysical Research: Atmospheres **124** (2019) 1720. https://doi.org/10.1029/2018JD028878.

[13] A. B. M. Collow, M. A. Miller, L. C. Trabachino, M. P. Jensen & M. Wang, "Radiative heating rate profiles over the southeast Atlantic Ocean during the 2016 and 2017 biomass burning seasons", Atmospheric Chemistry and Physics **20** (2020) 10073. https://doi.org/10.5194/acp-20-10073-2020.

[14] S. Ramachandran, M. Rupakheti & M. G. Lawrence, "Aerosol - induced atmospheric heating rate decreases over South and East Asia as a result of changing content and composition", Scientific Reports **10** (2020) 1. https://doi.org/10.1038/s41598-020-76936-z.

[15] C. M. Liu & S. S. Ou, "Effects of tropospheric aerosols on the solar radiative heating in a clear atmosphere", Theoretical and Applied Climatology **41** (1990) 97. https://doi.org/10.1007/BF00866432

[16] M. Mallet, P. Tulet, D. Serça, F. Solmon, O. Dubovik, J. Pelon, V. Pont & O. Thouron, "Impact of dust aerosols on the radiative budget, surface heat fluxes, heating rate profiles and convective activity over West Africa during March 2006", Atmospheric Chemistry and Physics **9** (2009) 7143. https://doi.org/10.5194/acp-9-7143-2009

[17] C. Lemaître, C. Flamant, J. Cuesta, J. C. Raut, P. Chazette, P. Formenti & J. Pelon, "Radiative heating rates profiles associated with a springtime case of Bodélé and Sudan dust transport over West Africa", Atmospheric Chemistry and Physics **10** (2010) 8131. https://doi.org/10.5194/acp-10-8131-2010.

[18] P. Pilewskie, J. Pommier, R. Bergstrom, W. Gore, S. Howard, M. Rabbette, B. Schmid, P. V. Hobbs & S. C. Tsay, "Solar spectral radiative forcing during the Southern African Regional Science Initiative", Journal of Geophysical Research **108** (2003) 1. https://doi.org/10.1029/2002JD002411.

[19] P. Kokkalis, O. Soupiona, C. Papanikolaou, R. Foskinis, M. Mylonaki, S. Solomos, S. Vratolis, V. Vasilatou, E. Kralli, D. Anagnou & A. Papayannis, "Radiative effect and mixing processes of a long-lasting dust event over athens, greece, during the COVID-19 period", Atmosphere. **12** (2021) 1. https://doi.org/10.3390/atmos12030318.

[20] C. Zhao, X. Liu, L. R. Leung, B. Johnson, S. A. McFarlane, W. I. Gustafson Jr., J. D. Fast & R. Easter, "The spatial distribution of mineral dust and its shortwave radiative forcing over North Africa: Modeling sensitivities to dust emissions and aerosol size treatments", Atmospheric Chemistry and Physics **10** (2010) 8821. https://doi.org/10.5194/acp-10-8821-2010.

[21] F. Malavelle, V. Pont, M. Mallet, F. Solmon, B. Johnson, J. F. Leon & C. Liousse, "Simulation of aerosol radiative effects over West Africa during DABEX and AMMA SOP - 0", Journal of Geophysical Research **116** (2011) 1. https://doi.org/10.1029/2010JD014829.

[22] J. W. Makokha, J. O. Odhiambo & J. G. Shem, "Long Term Assessment of Aerosol Radiative Forcing over Selected Sites of East Africa", Journal of Geoscience and Environment Protection **6** (2018) 22. https://doi.org/10.4236/gep.2018.64002.

[23] K. R. Kumar, R. Boiyo, R. Khan, N. Kang, X. Yu, V. Sivakumar, D. Griffith & N. L. Devi, "Multi-year analysis of aerosol optical properties and implications to radiative forcing over urban Pretoria, South Africa", Theoretical and Applied Climatology **141** (2020) 343. https://doi.org/10.1007/s00704-020-03183-7.

[24] B. Pathak, G. Kalita, K. Bhuyan, P. K. Bhuyan & K. K. Moorthy, "Aerosol temporal characteristics and its impact on shortwave radiative forcing at a location in the northeast of India", Journal of Geophysical Research: Atmospheres **115** (2010) D19204. https://doi.org/10.1029/2009JD013462

[25] T. Nishizawa, S. Asano, A. Uchiyama & A. Yamazaki, "Seasonal variation of aerosol direct radiative forcing and optical properties estimated from ground-based solar radiation measurements", Journal of Atmospheric Sciences **61** (2004) 57. https://doi.org/10.1175/1520-0469(2004)061(0057)2.0.CO;2.

[26] C. K. Peng, S. V. Buldyrev, S. Havlin, M. Simons, H. E. Stanley & A. L. Goldberger, "Mosaic organizations of DNA nucleotides", Physical Review E **49** (1994) 1685. https://doi.org/10.1103/PhysRevE.49.1685.

[27] S. Damouras, M. D. Chang, E. Sejdić & T. Chau, "An empirical examination of detrended fluctuation analysis for gait data", Gait & Posture **31** (2010) 336. https://doi.org/10.1016/j.gaitpost.2009.12.002.

[28] D. Chen & H. W. Chen, "Using the Köppen classification to quantify climate variation and change: an example for 1901–2010", Environmental Development **6** (2013) 69. https://doi.org/10.1016/j.envdev.2013.03.007.

[29] T. Igbawua, M. Hembafan & F. Ujoh, "Suitability analysis for yam production in Nigeria using satellite and observation data", Journal. Nigerian Society of Physical Science **4** (2022) 883. https://doi.org/10.46481/jnsps.2022.883.

[30] Global Modeling and Assimilation Office (GMAO)**,** "tavgM_2d_aer_Nx: MERRA-2 2D, Monthly Mean, Time-Averaged, Single-Level, Assimilated Aerosol Diagnostics (0.625x0.5), version 5.12.4." Greenbelt, MD, USA: Goddard Space Flight Center Distributed Active Archive Center (GSFC DAAC), 2015. [Online]. (Accessed November 1, 2022). https://doi.org/10.5067/FH9A0MLJPC7N.

[31] Global Modeling and Assimilation Office (GMAO), "tavgM_2d_rad_Nx: MERRA-2 2D, Monthly Mean, Time-Averaged, Single-Level, Radiation Diagnostics (0.625x0.5), version 5.12.4." Greenbelt, MD, USA: Goddard Space Flight Center Distributed Active Archive Center (GSFC DAAC), 2015. [Online]. (Accessed October 23, 2023). https://doi.org/10.5067/OU3HJDS973O0.

[32] Global Modeling and Assimilation Office (GMAO), "instM_2d_gas_Nx: MERRA-2 2D, Monthly Mean, Single-Level, Assimilated Gas Diagnostics (0.625x0.5), version 5.12.4." Greenbelt, MD, USA: Goddard Space Flight Center Distributed Active Archive Center (GSFC DAAC), 2015. [Online]. (Accessed June 20, 2022). https://doi.org/10.5067/XOGNBQEPLUC5.

[33] J. W. Kantelhardt, E. Koscielny-Bunde, H. H. A. Rego, S. Havlin & A. Bunde, "Detecting long-range correlations with detrended uctuation analysis", Physica A **295** (2001) 441. https://doi.org/10.1016/S0378-4371(01)00144-3.

[34] G. W. Khamala, J. W. Makokha, R. Boiyo & K. R. Kumar, "Spatiotemporal analysis of absorbing aerosols and radiative forcing over environmentally distinct stations in East Africa during 2001–2018", Science of the Total Environment **864** (2023) 161041. https://doi.org/10.1016/j.scitotenv.2022.161041.

[35] S. S. Aladodo, C. O. Akoshile, T. B. Ajibola, M. Sani, O. A. Iborida & A. A. Fakoya, "Seasonal tropospheric aerosol classification using AERONET spectral absorption properties in African locations", Aerosol Sci Eng. **6** (2022) 246. https://doi.org/10.1007/s41810-022-00140-x.

[36] N. A. Caserini & P. Pagnottoni, "Effective transfer entropy to measure information flows in credit markets", Statistical Methods & Applications **31** (2022) 729. https://doi.org/10.1007/s10260-021-00614-1.

[37] H. B. Mann, "Nonparametric tests against trend", Econometrica: Journal of the Econometric Society **13** (1945) 245. https://doi.org/10.2307/1907187.

[38] M. G. Kendall, *Rank correlation methods*, Griffin, London, UK, 1948. https://psycnet.apa.org/record/1948-15040-000.

[39] M. A. Balarabe, F. Tan, K. Abdullah & M. N. M. Nawawi, "Temporalspatial variability of seasonal aerosol index and visibility–a case study of Nigeria", presented at International Conference on Space Science and Communication (IconSpace), Langkawi, Malaysia, 2015. [Online]. https://doi.org/10.1109/IconSpace.2015.7283769.

[40] P. Tian, D. Liu, D. Zhao, C. Yu, Q. Liu, M. Huang, Z. Deng, L. Ran, Y. Wu, S. Ding, K. Hu, G. Zhao & C. Zhao, "In situ vertical characteristics of optical properties and heating rates of aerosol over Beijing", Atmospheric Chemistry and Physics **20** (2020) 2603. https://doi.org/10.5194/acp-20-2603-2020.

[41] V. S. Nair, S. S. Babu, M. R. Manoj, K. K. Moorthy & M. Chin, "Direct radiative effects of aerosols over South Asia from observations and modeling", Climate Dynamics **49** (2017) 1411. https://doi.org/10.1007/s00382-016-3384-0.

[42] M. Collaud Coen, E. Andrews, A. Alastuey, T. P. Arsov, J. Backman, B. T. Brem, N. Bukowiecki, C. Couret, K. Eleftheriadis, H. Flentje, M. Fiebig, M. Gysel-Beer, J. L. Hand *et al.*, "Multidecadal trend analysis of in situ aerosol radiative properties around the world", Atmospheric Chemistry and Physics **20** (2020) 8867. https://doi.org/10.5194/acp-20-8867-2020.

[43] A. K. Srivastava, S. Singh, S. Tiwari & D. S. Bisht, "Contribution of anthropogenic aerosols in direct radiative forcing and atmospheric heating rate over Delhi in the Indo-Gangetic Basin", Environmental Science and Pollution Research **19** (2012) 1144. https://doi.org/10.1007/s11356-011-0633-y.

[44] R. P. Guleria & J. C. Kuniyal, "Characteristics of atmospheric aerosol particles and their role in aerosol radiative forcing over the northwestern Indian Himalaya in particular and over India in general", Air Quality, Atmosphere & Health **9** (2016) 795. https://doi.org/10.1007/s11869-015-0381-0.

[45] J. L. Gómez-Amo, A. di Sarra & D. Meloni, "Sensitivity of the atmospheric temperature profile to the aerosol absorption in the presence of dust", Atmospheric Environment **98** (2014) 331. https://doi.org/10.1016/j.atmosenv.2014.09.008.

[46] A. K. Srivastava, B. J. Mehrotra, A. Singh, V. Singh, D. S. Bisht, S. Tiwari & M. K. Srivastava, "Implications of different aerosol species to direct radiative forcing and atmospheric heating rate", Atmospheric Environment **241** (2020) 117820. https://doi.org/10.1016/j.atmosenv.2020.117820.

[47] S. Kumar & P. C. S. Devara, "A long-term study of aerosol modulation of atmospheric and surface solar heating over Pune, India", Tellus B: Chemical and Physical Meteorology **64** (2012) 18420. https://doi.org/10.3402/tellusb.v64i0.18420.

[48] H. Che, M. Segal-Rozenhaimer, L. Zhang, C. Dang, P. Zuidema, A. J. Sedlacek III & C. Flynn, "Seasonal variations in fire conditions are important drivers in the trend of aerosol optical properties over the southeastern Atlantic", Atmospheric Chemistry and Physics **22** (2022) 8767. https://doi.org/10.5194/acp-2022-160.

[49] L. Zhang, Z. Luo, W. Du, G. Li, G. Shen, H. Cheng & S. Tao, "Light absorption properties and absorption emission factors for indoor biomass burning", Environmental Pollution **267** (2020) 115652. https://doi.org/10.1016/j.envpol.2020.115652.

[50] J. Zhai, X. Lu, L. Li, Q. Zhang, C. Zhang, H. Chen & J. Chen, "Size-resolved chemical composition, effective density, and optical properties of biomass burning particles", Atmospheric Chemistry and Physics **17** (2017) 7481. https://doi.org/10.5194/acp-17-7481-2017.

[51] S. S. Raj, O. O. Kruger, A. Sharma, U. Panda, C. Pohlker, D. Walter, J. Forster, R. P. Singh, *et al.*, "Planetary boundary layer height modulates aerosol –water vapor interactions during winter in the megacity of delhi journal of geophysical research: atmospheres", Journal of Geophysical Research: Atmospheres **126** (2021) 1. https://doi.org/10.1029/2021JD035681.

[52] J. Zou, J. Sun, A. Ding, M. Wang, W. Guo & C. Fu, "Observation-based estimation of aerosol-induced reduction of planetary boundary layer height", Advances in Atmospheric Sciences **34** (2017) 1057. https://doi.org/10.1007/s00376-016-6259-8.

[53] H. Wang, Z. Li, Y. Lv, H. Xu, K. li, D. Li, W. Hou, F. Zheng, Y. Wei & B. Ge, "Observational study of aerosol-induced impact on planetary boundary layer based on lidar and sunphotometer in Beijing", Environmental Pollution **252** (2019) 897. https://doi.org/10.1016/j.envpol.2019.05.070.

[54] C. D. Roberts, M. D. Palmer, R. P. Allan, D. G. Desbruyeres. P. Hyder, C. Liu & D. Smith, "Surface flux and ocean heat transport convergence contributions to seasonal and interannual variations of ocean heat content", Journal of Geophysical Research: Oceans **122** (2016) 1. https://doi.org/10.1002/2016JC012278.

[55] J. Wang & J. A. Carton, "Seasonal heat budgets of the north pacific and north atlantic oceans", Journal of Physical Oceanography **32** (2002) 3474. https://doi.org/10.1175/1520-0485(2002)032%3c3474:SHBOTN%3e2.0.CO;2.

[56] M. R. Perrone, A. M. Tafuro & S. Kinne, "Dust layer effects on the atmospheric radiative budget and heating rate profiles", Atmospheric Environment **59** (2012) 344. https://doi.org/10.1016/j.atmosenv.2012.06.012.